ACS APPLIED MATERIALS & INTERFACES

Research Article

www.acsami.org

Graphene/Cu Nanoparticle Hybrids Fabricated by Chemical Vapor Deposition As Surface-Enhanced Raman Scattering Substrate for Label-Free Detection of Adenosine

Shicai Xu,*[,†] Baoyuan Man,[‡] Shouzhen Jiang,[‡] Jihua Wang,[†] Jie Wei,[§] Shida Xu,[∥] Hanping Liu,[†] Shoubao Gao,[‡] Huilan Liu,[†] Zhenhua Li,[†] Hongsheng Li,[⊥] and Hengwei Qiu[‡]

[†]College of Physics and Electronic Information, Shandong Provincial Key Laboratory of Functional Macromolecular Biophysics, Institute of Biophysics, Dezhou University, Dezhou 253023, China

[‡]College of Physics and Electronics, Shandong Normal University, Jinan 250014, China

[§]Department of Neurology, Dezhou People's Hospital, Dezhou 253014, China

[∥]Department of Internal Medicine, Dezhou People's Hospital, Dezhou 253014,China

[⊥]Department of Radiation Oncology, Key Laboratory of Radiation Oncology of Shandong Province, Shandong Cancer Hospital and Institute, Jinan 250117, China

Supporting Information

ABSTRACT: We present a graphene/Cu nanoparticle hybrids (G/CuNPs) system as a surface-enhanced Raman scattering (SERS) substrate for adenosine detection. The Cu nanoparticles wrapped by a monolayer graphene shell were directly synthesized on flat quartz by chemical vapor deposition in a mixture of methane and hydrogen. The G/CuNPs showed an excellent SERS enhancement activity for adenosine. The minimum detected concentration of the adenosine in serum was demonstrated as low as 5 nM, and the calibration curve showed a good linear response from 5 to 500 nM. The capability of SERS detection of adenosine in real normal human urine samples based on G/CuNPs was also investigated and the characteristic peaks of adenosine were still recognizable. The reproducible and the ultrasensitive enhanced Raman signals could be due to the presence of an ultrathin graphene layer. The graphene shell was able to enrich and fix the adenosine molecules, which could also efficiently maintain chemical and optical stability of G/CuNPs. Based on the G/CuNPs system, the ultrasensitive SERS detection of adenosine in varied matrices was expected for the practical applications in medicine and biotechnology.

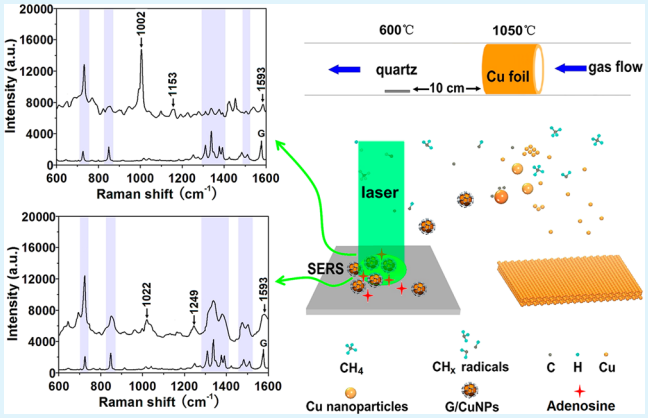

KEYWORDS: *graphene, Cu nanoparticles, CVD, SERS, adenosine detection*

INTRODUCTION

In recent decades, surface-enhanced Raman spectroscopy as a very important analytical technique for biomedical detection has received increasing attention.[1−3] As a widely used method, SERS shows its unique and excellent properties for the biological system. Although Raman spectroscopy is limited by low sensitivity, SERS could provide signal intensity of the molecules enhanced by orders of magnitude on the proper substrates. During the past decades, metallic nanomaterials, such as Ag, Au, and Cu nanoparticles, as SERS-active substrates have been widely reported.[4] Numerous attempts have been done to design well-ordered Ag or Au nanostructures with high SERS activity.[4,5] Despite considerable efforts, it is still a challenge to achieve ideal SERS substrates with good stability and reproducibility.[6] Actually, the issue of metal−molecule contact induced signal variations has become a key problem for practical applications.[7,8] Furthermore, the lower adsorption capacity of metal nanostructures for some molecules often limits their applications.[9]

Using a thin and pinhole free layer of SiO_2 or Al_2O_3 as an inert shell to isolate metal nanostructures from their surroundings was demonstrated,[7] but the approach is challenging for a normal metal substrate. Fabrication of SERS substrates with an ultrathin passivated surface at a lowest loss of electromagnetic enhancement activity is the key to shell-isolated SERS. The main challenge is to get a pinhole-free coating layer with a very small thickness. The atomic thickness and seamless structure of graphene makes it a natural candidate

Received: March 16, 2015
Accepted: May 5, 2015
Published: May 5, 2015

DOI: 10.1021/acsami.5b02303
ACS Appl. Mater. Interfaces 2015, 7, 10977−10987

material for shell-isolated SERS. Graphene, a 2D atomic crystal with densely packed carbon atoms in a honeycomb crystal lattice,[10] is well-known for its unique electrical performance and the amazing applications in nanoscale electronics.[11] As well as the wide interest in its electric properties, graphene is also a rising star in Raman spectroscopy.[12] An atomic flat surface of graphene causes a small-distance charge transfer between the graphene surface and adsorbed molecules, making the Raman signal more reliable and efficient. Beside the ultrathin structure, graphene also has a large specific surface area of 2630 m^2/g,[13] which can act as an excellent adsorbent toward organic molecules, especially the aromatic molecules. Therefore, graphene can also work as a molecule enricher in SERS-active substrate.[14,15] It has been reported that graphene can effectively enhance the Raman signal and reduce the background noise.[16,17]

Recently, many studies have been done to obtain graphene−noble metallic nanomaterials for SERS. These hybrids show great promise for applications in SERS. Zhang et al. reported a one-pot route to prepare SERS substrate by employing single-layer Ag−graphene composite nanosheets hybrid materials.[18] He et al. demonstrated that the gold decorated graphene can serve as a SERS-active substrate for multiplexing detection of DNA.[19] Xie et al. reported a SERS sensor based on graphene and silver composite which can detect prohibited colorants in food.[20] Zhao et al. fabricated a kind of highly SERS-active substrate by employing highly dispersed Ag on graphene nanosheets.[21] Iliut et al. reported a green approach for synthesis of Au−graphene hybrids as SERS platforms.[22] Liu and Chen synthesized graphene nanosheets-supported Ag nanoparticles as SERS substrate for detection of TNT.[23] Lu et al. obtained high sensitivity surface enhanced Raman spectroscopy of R6G on in situ fabricated Au nanoparticle/graphene plasmonic substrates.[24] These works provided facile methods to decorate metal nanoparticles on the surface of graphene on which the graphene can be an effective molecule enricher. However, the adopted graphene layer in these methods did not essentially isolate the probed materials from the metallic Raman reporters. To solve this problem, Xu et al. prepared a graphene-veiled gold substrate with a passivated surface for SERS.[25] Xie's group fabricated a hybrid SERS-active platform consisting of a single layer graphene (SLG) covering a quasiperiodic Au nanopyramid and showed a very high SERS enhancement factor of over 10^{10} for rhodamine 6G (R6G).[26] Zhu's group has shown that graphene−gold nanoparticle hybrid films are a promising material for shell isolated SERS.[27] Li et al. fabricated monolayer graphene-covered Ag nanoparticles by transfer method and demonstrated that the graphene layer can obviously suppress the oxidation of Ag nanoparticles.[28] More reproducible SERS signals were demonstrated in these studies by employing graphene as the passivated surface. Nevertheless, there is still a principal disadvantage in signal stability and reproducibility for these methods. As in all the above-mentioned methods, the graphene−metal hybrids were obtained either through transferring a graphene sheet on the surface of metal nanoparticles or spin-coating a mixed solution of graphene and metal nanoparticles. As both approaches essentially belong to physical composition, the tightly sealed structure is hard to form between metallic nanoparticles and graphene shell. The space between graphene and metal nanoparticles will inevitably cause apparent loss of electromagnetic enhancement activity as the electromagnetic enhancement efficiency decays rapidly with distance between the metal nanoparticles and analytes. Moreover, the suspended and wrinkled graphene structures always formed near the gaps of nanoparticles,[26,28] making graphene−metal hybrids nonuniform and easy to damage, further reducing the homogeneity and reproducibility of the SERS substrates. It is satisfactory to use chemical vapor deposition (CVD) method to directly grow a thin layer of graphene on the surface of nanoparticles. However, it is very difficult to grow high quality graphene on the Au or Ag substrate. High quality graphene can be grown on Cu foil at the high temperature of ∼1000 °C.[29] While for Cu nanoparticles, due to the small size effect, they can not withstand the high graphene growth temperature, at which these nanoparticles will almost be vaporized or at least completely melted depending on their original shape and size. Thus, it is desired to develop a new way to grow graphene layer on Cu nanoparticles to fabricate Cu−graphene SERS substrates with good stability and reproducibility.

In this work, we provide a direct growth approach to prepare a high performance SERS substrate with graphene-wrapped Cu nanoparticles by a two-temperature-zone CVD method. As a chemistry composite mode, this method provides an atomically thin, seamless, and chemically inert net to tightly wrap the metallic nanoparticles. Compared with previously reported works, this approach exhibits three advantages. First, the direct growth mode make graphene layer tightly wrap the metal nanoparticles, minimize the loss of electromagnetic enhancement activity. Second, the direct grown graphene shell is free from suspended and wrinkled structures and effectively avoids graphene damage, thus providing enhanced chemical stability and reproducibility of SERS. Third, direct grown graphene can cover every place of the G/CuNPs, even the narrow gaps of particles (hot spots). So the target molecules can be more effectively absorbed on the hot spots, and thus more sensitive Raman signals are expected. Based on the G/CuNPs, ultrasensitive and label-free detection of adenosine by SERS spectra was demonstrated. Adenosine, a metabolite of adenine nucleotides, is one of the major neuromodulators. Adenosine has been recognized as an endogenous anticonvulsant and neuroprotective molecule. As the core molecule of ATP and of nucleic acids, adenosine forms a unique link among cell energy, gene regulation, and neuronal excitability.[30] Adenosine has long been a highly coveted therapeutic target, and its actions at the A1 receptor subtype hold well-established and profound therapeutic potential for conditions such as stroke, brain injury, pain, and epilepsy, among others.[31,32] Adenosine also has drawn attention as possible tumor markers in human cancers, because adenosine level in cancer patients is generally found to be significantly higher than that in healthy person.[33−35] Therefore, it is interesting to develop a highly specific and sensitive method for adenosine detection. On the basis of the G/CuNPs, low limit of detection was achieved in water, serum and normal human urine by SERS. The successful collection of clean and reproducible adenosine SERS signals in varied matrices indicated that the G/CuNPs substrate have great potential for detection application in medicine and biotechnology field.

RESULTS AND DISCUSSION

The prime feature of the proposed approach include fabrication of Cu nanoparticles (CuNPs) by remote thermal evaporation and the direct formation of graphene layer on the surface of CuNPs in the mixture of Cu vapor, H, and decomposed CH_4. Figure 1a shows the growth setup of G/CuNPs. The CVD hot-

DOI: 10.1021/acsami.5b02303
ACS Appl. Mater. Interfaces 2015, 7, 10977−10987

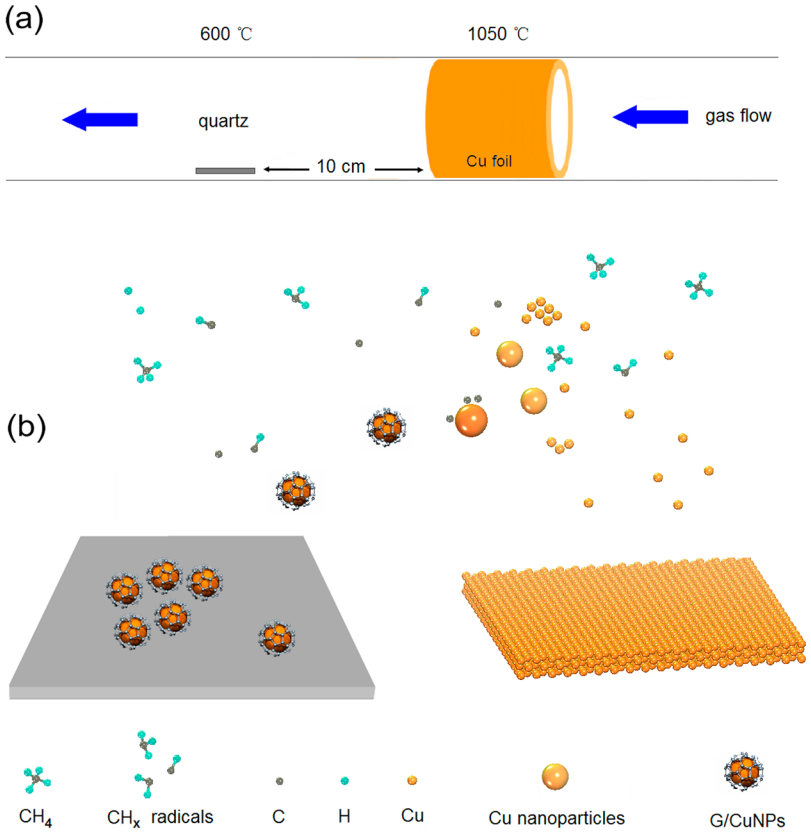

Figure 1. (a) Growth setup. A strip of Cu foil surrounding along the tube wall was used to supply Cu nanoparticles as a floating catalyst. The quartz substrate was placed 10 cm away from the Cu strip. (b) Schematic illustration of graphene growth mechanism involving decomposition of CH_4 by floating Cu and H. Cu atoms are subliming from the Cu foil at 1050 °C and evolve into Cu nanoparticles at a certain concentration. Graphene starts growing on Cu nanoparticles in the mixture of H_2 and CH_4.

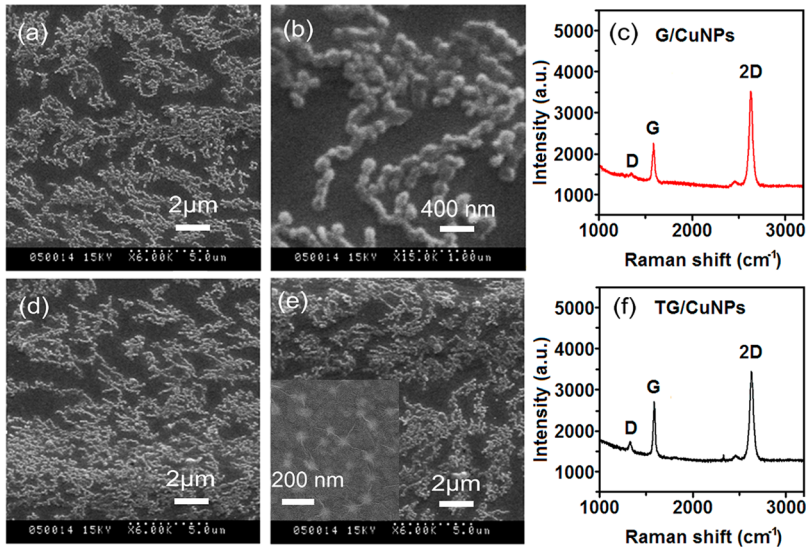

Figure 2. SEM images of G/CuNPs, CuNPs, and TG/CuNPs and Raman spectra of G/CuNPs and TG/CuNPs on a quartz substrate. (a) SEM image of G/CuNPs at a low magnification. (b) SEM image of G/CuNPs at a higher magnification. (c) Raman spectrum of G/CuNPs. (d) SEM image of CuNPs grown on a quartz substrate. (e) SEM image of TG/CuNPs on a quartz substrate. (f) Raman spectrum of TG/CuNPs.

wall reactor was designed with two temperature zones in which the temperature can be controlled independently. For G/CuNPs growth, the reactor was set with one zone at 600 °C and the other at 1050 °C. A strip of Cu foil cleaned by acetic acid surrounding along the tube wall was placed in the high-temperature zone in the upstream gas flow to supply CuNPs and achieve graphene growth in a mixture of H_2 and CH_4. The quartz substrates were placed in the low-temperature zone downstream at ∼10 cm away from the Cu foils for G/CuNPs deposition. Figure 1b schematically illustrates the working mechanism of the graphene growth on the surface of CuNPs. The Cu foil sublimes and produces a large number of Cu atoms

DOI: 10.1021/acsami.5b02303
ACS Appl. Mater. Interfaces 2015, 7, 10977−10987

at the high temperature of 1050 °C at low pressure of 280 Pa. When the Cu atoms attain a certain concentration, these Cu atoms begin to merge with each other, evolving into Cu nanoparticles with a certain size. On the other hand, the Cu atoms are also used as catalysts to decomposes CH_4, enabling a typically CVD reaction to grow a graphene layer on floating CuNPs. The graphene-wrapped Cu nanoparticles are then transported downstream with gas flow into the low-temperature zone, forming G/CuNPs structure on quartz substrates. As a comparison, we also prepared single CuNPs in the mixture of H_2 and Ar. The traditional CVD graphene grown on Cu foil were also transferred on the Cu nanoparticles, making the transferred graphene/Cu nanoparticle hybrids (TG/CuNPs). The detailed description of the experiment process can be found in the methods.

A scanning electron microscope (SEM) was used to investigate the surface morphology of G/CuNPs formed on the quartz substrate. Figure 2a shows the image of the sample at a low magnification. The quartz substrate is covered by a large number of nanoparticles with uniform size. To identify the size of nanoparticles, a higher magnification was adopted. As shown in Figure 2b, the average size of these nanoparticles is ∼100 nm and the gaps among nanoparticles are very narrow. Since metallic nanoparticles with narrow gaps are regarded to be essential for large Raman enhancement,[36] the narrow gaps are expected to support huge electromagnetic enhancement for absorbed molecules. As the direct grown graphene layer cannot be directly recognized by SEM observations, a conventional Raman measurement was performed on these nanoparticles to demonstrate the existence of graphene. As shown in Figure 2c, the D, G, and 2D peaks of graphene are clearly observed at ∼1360, ∼1580, and ∼2695 cm^{-1}, respectively. These peaks can be regarded as the fingerprint of graphene.[37,38] The Raman spectrum shows typical features of monolayer graphene: the intensity ratio of $I_{(2D)}/I_{(G)} \geq 2$ and a single Lorentzian 2D peak with a full width at half-maximum of 30−40 cm^{-1}.[29,39] Here, the defect-related D peak is very weak, indicative of high quality of graphene. These results demonstrate that the graphene film with a monolayer structure is actually grown on nanoparticles. By replacing the mixture of H_2 and CH_4 by H_2 and Ar, the single CuNPs are also formed on the quartz substrates (Figure 2d). The distribution of the CuNPs has not much difference with that of G/CuNPs from a statistical point of view. Also, the size of CuNPs is similar to that of G/CuNPs from the following TEM analysis. As a control experiment, we also fabricated TG/CuNPs by transferring a piece of CVD Cu foil based-graphene on the CuNPs. As shown in Figure 2e, the boundaries of nanoparticles become blurred after adding the graphene layer. In fact, because of the large fluctuation of the nanoparticles, the transferred graphene film had difficulty in getting closer to the surface of nanoparticles.[40] As shown in the inset of Figure 2e, the suspended and wrinkled graphene are formed on the edge of the nanoparticles. These suspended and wrinkled graphene structures were also appeared in the SEM image of graphene/nanapaticals hybrids in previous studies.[26,28] It is anticipated that these suspended and wrinkled graphene structure make the electromagnetic "hot" spots large distance from adsorbates and will cause apparent loss of electromagnetic enhancement active. On the other hand, the suspended structure can be damaged more easily, further resulting in the inhomogeneity of SERS substrates. Figure 2f shows the Raman spectrum collected from the TG/CuNPs. The typical graphene peaks are also observed. However, compared to the Raman spectrum of the as-grown graphene in the G/CuNPs, the defect-related D peak is much higher. The high level of defect can be attributed to the transfer damage caused in the graphene transfer process.

High resolution transmission electron microscopy (HRTEM) was employed to identify the exact dimensions of the G/CuNPs. Figure 3a shows the bright-field TEM image of

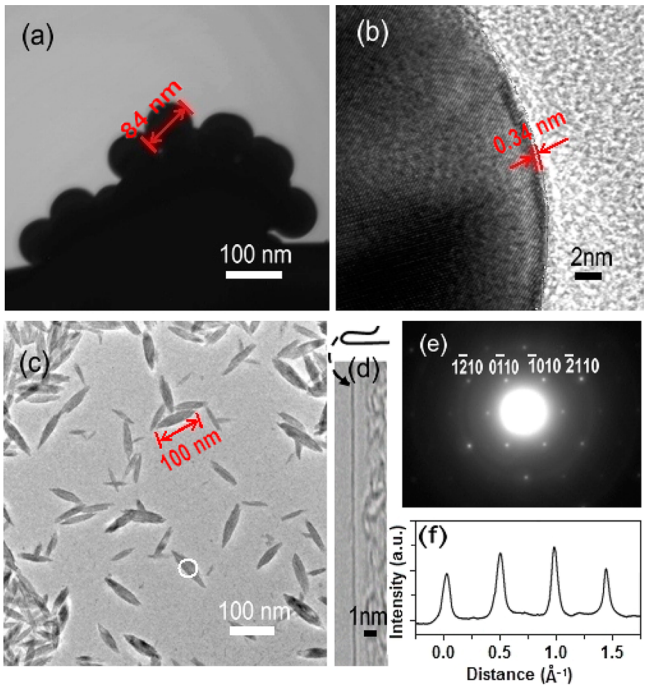

Figure 3. HRTEM images of G/CuNPs. (a) Bright-field TEM image of G/CuNPs. (b) HRTEM image of cross section of a graphene film grown on Cu nanoparticles. (c) Bright-field TEM of the graphene shell after removing the Cu nanoparticles. (d) TEM images of folded edges for monolayer graphene. (e) Electron diffraction patterns taken from the positions of the graphene sheet marked by white spots in (c). (f) Diffracted intensity taken along the $1\bar{2}10$ to $\bar{2}110$ axis on the patterns shown in (e).

G/CuNPs. The as-prepared nanoparticles are spherical shape with an average diameter of ∼80 nm. The sizes of the CuNPs were also observed by TEM as shown in Figure S1 in the Supporting Information (SI). Though the background gases are different, the grown CuNPs have similar shape and size with G/CuNPs, which is an important factor for control group of TG/CuNPs. Considering electromagnetic enhancement efficiency decays rapidly with distance R between donor and acceptor under a $1/R^{12}$ or $1/R^{10}$.[41] The ultrathin shell is a key factor for generating high SERS activity. In order to identify the thickness of the graphene shell, very detailed structural information of a nearby interface was captured by cross section HRTEM image of G/CuNPs (Figure 3b). It is apparent that Cu particles are covered by an ultrathin film, suggesting the formation of graphene-wrapped Cu nanoparticle hybrids. The shell layer is about 0.34 nm in thickness, indicative of monolayer graphene.[10] The graphene layer can be further characterized by removing the Cu nanoparticles in 0.5 M $FeCl_3$ solution. As shown in Figure 3c, lance-shaped graphene sheets are observed in bright-field TEM of the graphene sheet after removing the Cu nanoparticles. This result can be understood by considering that the spherical-graphene shell can not be self-supported after removing the inner Cu nanoparticles. The average size of the

DOI: 10.1021/acsami.5b02303
ACS Appl. Mater. Interfaces 2015, 7, 10977−10987

lance-shaped graphene sheet is ~100 nm, slightly lager that that of the G/CuNPs. This phenomenon can be attributed to the geometry change of graphene shell. A HRTEM analysis of folds at the edges of lance-shaped graphene sheet can give the number of graphene layers by direct visualization. The number of dark lines represents the number of graphene layer.[42] As shown in Figure 3d, the HRTEM image derived from the edge of the lance-shaped graphene sheet exhibits only one dark line, indicative of monolayer graphene. Figure 3e shows the SAED patterns of the graphene sheet. Typical 6-fold symmetry patterns are observed from the region marked with the white circle in Figure 3c, indicating the single-crystalline nature of the observed domain.[43] For further quantitative analysis of diffraction patterns, we labeled the peaks with Bravais-Miller indices. As shown in Figure 3f, the inner peaks $(0\bar{1}10)$ and $(\bar{1}010)$ are more intense than the outer ones $(1\bar{2}10)$ and $(\bar{2}110)$, further confirming monolayer nature of the graphene.[44]

XPS is a kind of surface sensitive technique to analyze the chemical composition. Figure 4a shows the full XPS spectrum

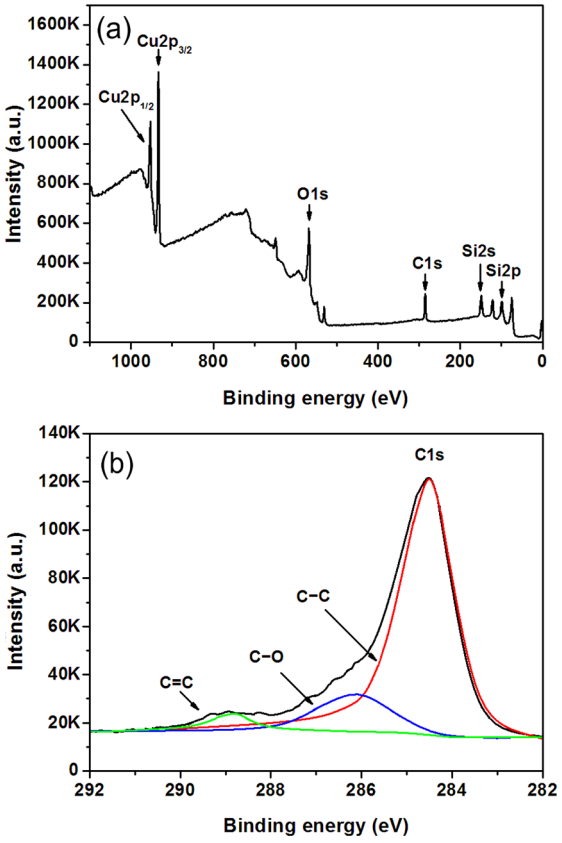

Figure 4. XPS spectra of G/CuNPs on quartz substrates. (a) Full XPS spectrum of G/CuNPs on quartz substrates. (b) Detailed C 1s core-level spectrum of graphene shell on Cu nanoparticles. Curve fitting of the spectrum was carried out using a Gaussian–Lorentzian peak shape.

of G/CuNPs on quartz substrates. The characteristic peaks from Cu high are clearly observed at ~935 and ~952 eV, indicating the formation of Cu nanoparticles.[45] The signals of O 1s at ~532 eV, Si 2s at and Si 2p at ~105.1 eV are assigned to quartz substrate.[45,46] The distinct peak of C 1s at ~284 eV is the signature of sp^2 C–C network, consistent with the formation of graphene.[47] Figure 4b shows the detailed C 1s core-level spectrum of G/CuNPs. The C 1s can be deconvolved into three components. The main peak at 284.5 eV indicates the formation of a sp^2 C–C network for the grown film.[48] The discernible tail at 286.3 and 288.9 eV is assigned to the hydroxyl carbon C–O and C═O, respectively.[47] The higher energy C 1s peaks related to carbon–oxygen bonds are often observed in the CVD grown graphene, which is probably due to the oxygen contamination inside of the growth chamber. In a further comparison with transferred gaphene on SiO_2,[49] the C 1s peak exhibits a slight blueshift (from 284.4 to 284.5 eV). We suppose that weak chemical bonding interaction between graphene and CuNPs causes descreening of nucleus charges, leading to an overall increase in core electron binding energies.

To estimate the SERS activity of the G/CuNPs, 10^{-6} M aqueous solution of adenosine was chosen as the probe molecule. The SERS spectra of adenosine on the TG/CuNPs and CuNPs were also collected as the contrast. As shown in Figure 5a, three sets of peaks are observed on the SERS spectra

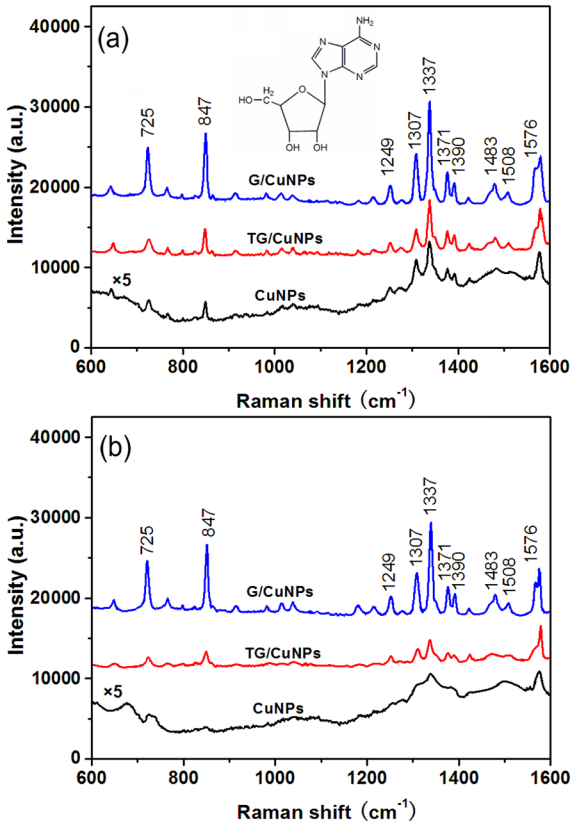

Figure 5. (a) Comparison of SERS spectra of adenosine on G/CuNPs, TG/CuNPs, and CuNPs. Inset: the structural formula of adenosine molecule. (b) Comparison of SERS spectra of adenosine on G/CuNPs, TG/CuNPs, and CuNPs after oxidation treatment.

of adenosine on three kinds of SERS substrates. The primary vibrations of adenosine are confirmed according to the reported work.[50−53] It is distinct that the intensities of SERS spectra on G/CuNPs are much stronger than those of TG/CuNPs or CuNPs. The peaks at 725, 1483, 1508, and 1576 cm^{-1} assigned to the ring breathing modes of the whole molecule from G/CuNPs are about 2–5 times stronger than that of TG/CuNPs and 15–20 times stronger than that of CuNPs. The peak at 847 cm^{-1} assigned to skeletal mode of C–O–C from G/CuNPs is ~2.5 times stronger than that from TG/CuNPs and ~17.5 times stronger than that from CuNPs. The peak at 1307 cm^{-1}

DOI: 10.1021/acsami.5b02303
ACS Appl. Mater. Interfaces 2015, 7, 10977–10987

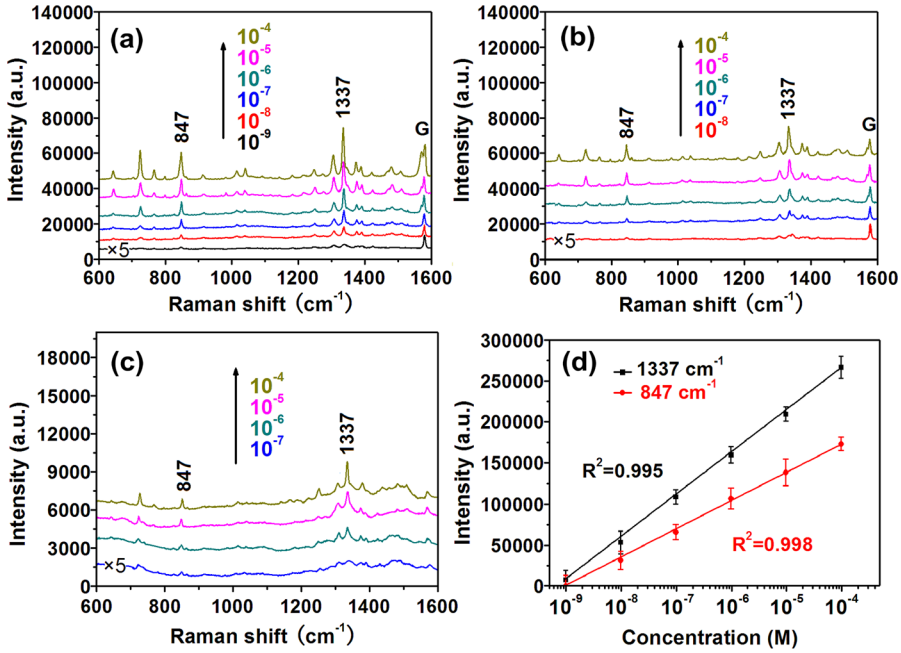

Figure 6. (a) Raman spectra of adenosine on G/CuNPs with different concentrations from 10^{-9} to 10^{-4} M. (b) Raman spectra of adenosine on TG/CuNPs with different concentrations from 10^{-8} to 10^{-4} M. (c) Raman spectra of adenosine on CuNPs with different concentrations from 10^{-7} to 10^{-4} M. (d) Raman intensity of adenosine peaks at 847 and 1337 cm^{-1} on G/CuNPs, as a function of the adenosine molecular concentration with the high coefficient of determination (R^2) of 0.995 and 0.998, respectively.

assigned to the stretching vibration of N−C−N and C−C−N from G/CuNPs is ∼2.2 times stronger than that from TG/CuNPs and ∼11.3 times stronger than that from CuNPs. The peaks at 1249 and 1337 cm^{-1} assigned to the stretching vibration of C−N and the bending vibration of C−H from G/CuNPs are ∼2.2 times stronger than that from TG/CuNPs and ∼13.6 times stronger than that from CuNPs. The peak at 1371 cm^{-1} assigned to bending vibration of C−H and N−H and the stretching vibration of C−N from G/CuNPs is ∼2.0 times stronger than that from TG/CuNPs and ∼12.1 times stronger than that from CuNPs. The peak at 1390 cm^{-1} assigned to CH rocking from G/CuNPs is ∼1.4 times stronger than that from TG/CuNPs and ∼8.8 times stronger than that from CuNPs. Obviously, the sharp characteristic peaks in SERS spectrum of adenosine from G/CuNPs exhibits the best signal-to-noise ratio. Compared to the CuNPs, the graphene-wrapped CuNPs, both G/CuNPs and TG/CuNPs have better SERS activity. The additional enhancement of the SERS signal of adenosine on graphene-wrapped CuNPs can be attributed to the molecule enrichment from graphene and graphene-derived CM enhancement. In a further comparison with TG/CuNPs, the better enhancement from G/CuNPs can be attributed to the tight combination between graphene and Cu nanoparticles. Because of the direct growth mode, the graphene is free from suspended and wrinkled structure and has more close contact with the inside nanoparticles. Since the electromagnetic enhancement decays rapidly with distance between metal and analyte,[41] the close contact structure makes target molecules closer to the surface and thus is more suitable for large SERS activity. On the other hand, the growth combination mode avoids the damages induced by the transfer process, the chemical enhancement mechanism from graphene associated with charge transfer effects are expected to be enhanced. Furthermore, we tested the stability of the SERS substrate based on G/CuNPs, TG/CuNPs, and CuNPs though a thermal oxidation treatment. The thermal oxidation treatment was implemented by expositing G/CuNPs, TG/CuNPs, and CuNPs to hot and humid air (temperature: 85 °C, humidity: 80%) for 240 h. As shown in Figure 5b, after the oxidation treatment, the SERS intensity of G/CuNPs the adenosine is nearly unchanged, indicating excellent chemical stability of G/CuNPs. For the TG/CuNPs, the SERS intensity of the adenosine is obviously decreased after oxidation treatment. While for the oxidation treated CuNPs, the SERS intensity of the adenosine become very weak and some of the characteristic peaks of adenosine are absent. It has been known that CuNPs are easily oxidized when it is exposed to air. The decrease of the Raman signals can be ascribed to the formation of copper oxides on the surface of Cu nanoparticles. This assumption was confirmed by X-ray diffraction (XRD), energy dispersive spectroscopy (EDS) measurements, and X-ray photoelectron spectroscopy analysis of the samples (Figure S2 and S3, SI) after the thermal oxidation stability test. As shown in the SI, Figure S2a, the typical peaks of Cu_2O (111) and CuO (111) are clearly observed for CuNPs.[54] For the TG/CuNPs, weak peaks of Cu_2O (111) and CuO (111) are also observed.[54] While for the G/CuNPs, the signal of CuO is absent. After the thermal oxidation treatment, the CuNPs coalesced into larger aggregates with the development of irregular shapes and rough surface, indicating serious oxidative damage (Figure S2b in the SI). The obvious oxygen increase in the EDS of TG/CuNPs and CuNPs might be another evidence for the formation of CuO (Figure S2c in the SI). XPS measurements of the samples also shows shakeup features at ∼945 and ∼965 eV for the Cu $2p_{3/2}$ and $2p_{1/2}$ core levels, which are evident and diagnostic of an open $3d^9$ shell of Cu (+2) (Figure S3, SI).[55]The formation of copper oxide on the surface of CuNPs increases the thickness of the passivation layer, which results in decreasing enhancement activity of samples. As oxygen gas and moisture cannot permeate through the graphene layer, the graphene can effectively protect metal

DOI: 10.1021/acsami.5b02303
ACS Appl. Mater. Interfaces 2015, 7, 10977−10987

from oxygen damage. The thermal stability comparison indicates that the grown graphene shell on CuNPs can more effectively suppress degradation of the metallic nanostructures in comparison with the transferred graphene shell. The grown graphene shell on CuNPs avoids suspended structure and transfer-induced damages on the graphene layer, exhibiting better antioxidant ability for SERS substrates.

To achieve a lower limit of detection, the strongest peaks located at 847 and 1337 cm^{-1} were chosen as the signature to determine the concentration of adenosine in the samples. SERS spectra of the adenosine in a series of concentrations tested on G/CuNPs, TG/CuNPs, and the CuNPs substrates are shown in Figure 6a–c, respectively. The intensities of the SERS spectra rise with the increasing concentrations of adenosine, suggesting that the intensities are proportional to the amount of adenosine molecules. The minimum concentration of adenosine detected from G/CuNPs was as low as 10^{-9} M, which is 1 order of magnitude lower than that from TG/CuNPs and 2 orders of magnitude lower than that from CuNPs. The adenosine detection limit based on G/CuNPs is also much lower than that of other reported SERS adenosine detection or other methods for adenosine detection.[56−59] These results indicate that ultrasensitive detection of adenosine can be achieved based on the G/CuNPs. The SERS intensity of the vibration located at 847 and 1337 cm^{-1} versus the concentration of adenosine are also plotted in Figure 6d. Possibly because of the nonuniformity of G/CuNPs, the standard deviations of the intensity for some concentrations are relatively large. Nonetheless, a good linear SERS response from 10^{-9} to 10^{-4} M of adenosine is obtained. The coefficient of determination (R^2) of the linear fit calibration curve for the peaks of 847 and 1337 cm^{-1} is reached 0.995 and 0.998, respectively. The linear SERS responses versus concentration of adenosine were also obtained on TG/CuNPs and CuNPs from 10^{-8} to 10^{-4} M and from 10^{-7} to 10^{-4}, respectively (Figure S4, SI). For both cases, the linear correlation between SERS spectra intensity and adenosine concentration are not as good as that collected on G/CuNPs (a much smaller R^2 than that from G/CuNPs shown in the SI, Figure S4). It is indicated that G/CuNPs can provide more reliability and stability SERS signals for adenosine detection. The improved stability of SERS signals can also be attributed to the additional grown graphene layer. Compared to the transferred graphene, the as-grown graphene are free from the suspended structure and transfer-induced damage, providing more uniform and effective adsorption site for adenosine.

To investigate the feasibility of the detection of adenosine in real biological samples, the adenosine from 5 to 500 nM was added to the diluted human serum (one percent of serum in water). Then the diluted serum containing adenosine was detected on G/CuNPs. The SERS spectra of adenosine in different concentrations in diluted serum are illustrated in Figure 7a. The intensities of the SERS spectra of adenosine are proportional to the concentration of the adenosine in diluted serum. Besides, the characteristic SERS spectra of adenosine in serum are quite similar to that in water with comparable intensity. There are only a few weak additional peaks in the spectrum derived from blank serum (black curve in Figure 7a). These weak additional peaks are attributed to the components in serum which do not disturb the recognition of adenosine. It can be deduced that the influence of the remaining protein in serum is almost ignorable in adenosine detection. The high selectivity of adenosine can be explained by the inherent

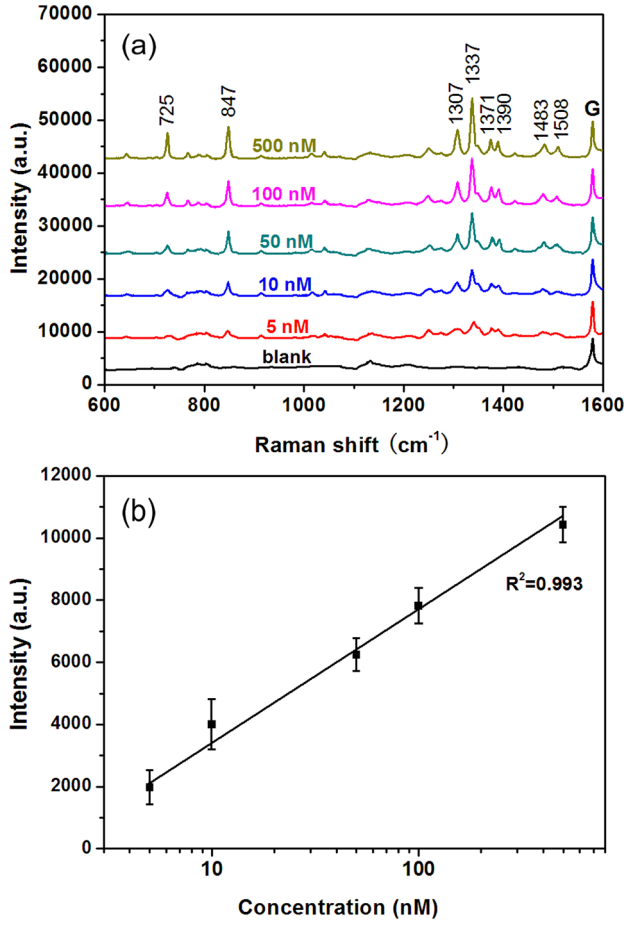

Figure 7. (a) Raman spectra of adenosine in diluted serum tested on G/CuNPs with different concentrations from 5 to 500 nM. (b) Raman intensity of adenosine in diluted serum at 1337 cm^{-1} on G/CuNPs, as a function of the adenosine concentration.

structure of adenosine and the binding interaction between adenosine and the G/CuNPs substrate. Compared to the complicated protein matrices in human serum, adenosine is a small molecule, and it can be more readily absorbed on the narrow gaps of nanoparticles (hot spots), and thus, more sensitive Raman signals are obtained. On the other hand, because of the heterocyclic aromatic structure of adenosine, the $\pi-\pi$ interactions of graphene–adenosine can serve as a strong driving force to bring adenosine in close proximity to hot spot of G/CuNPs, which can be another important factor for the high selectivity of adenosine.[15] The lowest detected concentration of adenosine in serum is 5 nM, corresponding to the spectrum (red curve in Figure 7a). To represent the capability of the quantitative detection of adenosine in serum and its reproducibility, the linear fit calibration curve (R^2 = 0.993) with error bars is illustrated in Figure 7b. The reasonable linear response of SERS is observed from 5 to 500 nM. The concentration gradient experiments of adenosine proved that the obtained G/CuNPs are good SERS substrates for the detection of adenosine in serum and the ignorable protein background indicates a potential application to detect adenosine in other practical biological systems.

As adenosine is also a possible tumor marker in human urine, we tested the normal human urine by using G/CuNPs. Figure 8a shows the SERS spectrum collected from human urine. The strong peaks at ~1002 cm^{-1} is assigned to symmetric ring

DOI: 10.1021/acsami.5b02303
ACS Appl. Mater. Interfaces 2015, 7, 10977−10987

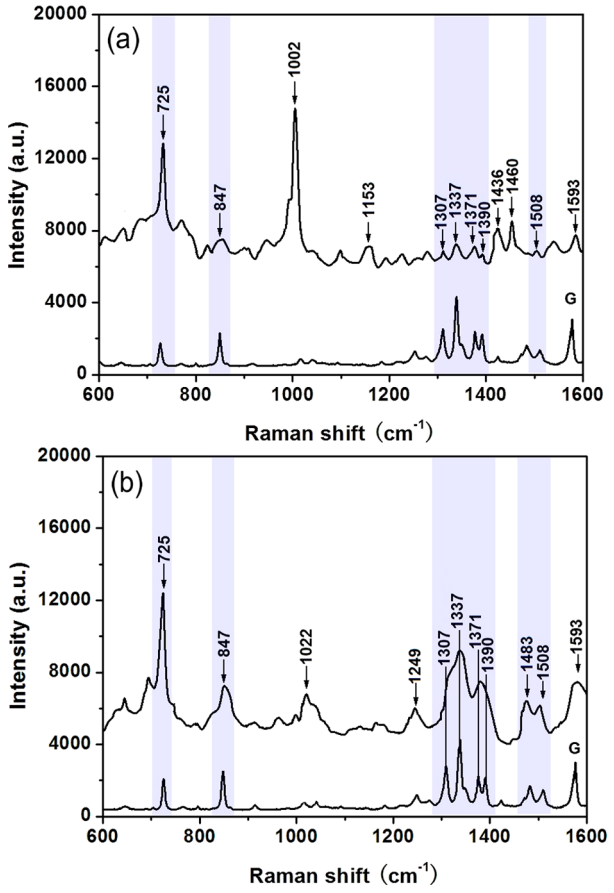

Figure 8. (a) Raman spectrum of normal human urine samples tested on G/CuNPs (top curve) and the Raman spectrum of adenosine with the concentration of 100 nM used as a reference (bottom curve). (b) Raman spectra of nucleosides excreted in a normal human urine sample tested on G/CuNPs (top curve) and the Raman spectra of adenosine with the concentration of 100 nM used as a reference (bottom curve).

breathing mode of phenylalanine.[60,61] The strong peak at ~1436 cm^{-1} is assigned to CH_2 scissoring of lipids and the one at ~1460 cm^{-1} is assigned to CH_2/CH_3 deformation lipids and collagen.[60,62] The strong peaks at ~1593 cm^{-1} is assigned to C═N, C═C stretching and ring stretches of phenylalanine.[63] The distinct peak at ~1153 cm^{-1} is assigned to carbohydrates for solutions.[53] It is worth noting that the adenosine related peaks at ~725, ~847, ~1307, ~1337, ~1371, ~1390, ~1483 and 1508 cm^{-1} can also be clearly recognized in the real human urine. The ~725 cm^{-1} assigned to ring breathing mode of adenosine is much enhanced, which can be attributed to the contribution of creatinine.[53] For adenosine detection in human urine, though some molecules such as phenylalanine also generate strong SERS signals, the characteristic signals of adenosine can still be clearly identified (Figure 8a). These interference signals can be explained by the fact that many molecules such as phenylalanine and some lipids also have aromatic structures and also have a good affinity to G/CuNPs substrate. More clear Raman peaks of adenosine can be obtained by extracting nucleosides from the urine samples. As shown in Figure 8b, the adenosine related peaks are much enhanced. As the adenosine excreted in the urine of patients with malignant tumors is usually in abnormal levels. The SERS spectra of adenosine obtained from G/CuNPs shows great potential in incipient cancer diagnosis and in the monitoring of therapeutic effects. However, the G/CuNPs based SERS substrate still needs to be improved for practical applications. It is expected to obtain a better reproducibility signal by improving the uniformity of nanoparticles by tuning the growth procedure of G/CuNPs. As the metallic silver has better plasma characteristics than copper, more sensitive SERS substrate is expected via replacing inner Cu nanoparticles by Ag nanoparticles. In fact, direct growth of monolayer graphene on metallic silver substrate is also possible by using solid carbon source according to the recent reports.[64] Further studies are now in progress in our group.

CONCLUSION

Herein graphene-wrapped Cu nanoparticle hybrids (G/CuNPs) were prepared as SERS substrates according to direct growth method. On the basis of the obtained G/CuNPs, an ultrasensitive and label-free SERS strategy was developed for the detection of adenosine in water, serum, and normal human urine according to the inherent SERS spectra of adenosine. The graphene shell was used to enrich and fix the adenosine molecules, on which reproducible and the ultrasensitive SERS signal of adenosine was obtained. The contrast of SERS spectra of adenosine on G/CuNPs, TG/CuNPs, and CuNPs showed that the direct graphene growth mode on CuNPs was very important for the ultrasensitivity and reproducibility of the SERS detection of adenosine. It was demonstrated that the minimum detected concentration of the adenosine in serum was as low as 5 nM, and the calibration curve showed a good linear relation with a linear response from 5 to 500 nM. The capability of SERS detection of adenosine in real normal human urine samples based on G/CuNPs was also investigated and the characteristic peaks of adenosine were still recognizable. The ultrasensitive SERS detection of adenosine in varied matrices was expected for the practical applications of G/CuNPs in medicine and biotechnology field.

EXPERIMENTAL SECTION

Fabrication of G/CuNPs on Flat Quartz Substrate. For G/CuNPs fabrication, the CVD hot-wall reactor was set with the low-temperature zone at 600 °C and the high-temperature zone at 1050 °C. A strip of Cu foil cleaned by acetic acid was placed surrounding along the tube wall in the high-temperature zone in the upstream gas flow to supply CuNPs. The graphene films were grown on the floating CuNPs by CVD process in a mixture of H_2 and CH_4. The quartz substrates were placed in the low-temperature zone downstream at ~10 cm away from the Cu foils for G/CuNPs deposition. After the vacuum reached a pressure of 10^{-5} Pa, the tube was rapidly heated up to 1050 °C with a rate of ~100 °C/min with flowing 50 sccm H_2 and 150 sccm Ar at 1350 Pa. The mixture of H_2 and CH_4 was used to remove the oxide layer on Cu foil and restrain the Cu evaporation during heating process. When the high-temperature zone reached 1050 °C, a mixture of 50 sccm H_2 and 10 sccm CH_4 was introduced into the tube to replace the mixture of H_2 and Ar at a low pressure of 280 Pa to start graphene growth. After 5 min CVD reaction, the G/CuNPs were deposited onto the flat quartz substrate in the low-temperature zone. Finally, the CH_4 was shut off and the quartz tube was rapidly cooled down to room temperature with flowing 50 sccm H_2 and 150 sccm Ar at 1350 Pa. The detailed experimental parameters were illustrated in Figure S5 in the SI. Unlike the self-limited growth mode on Cu foil, muti-layer graphene was

DOI: 10.1021/acsami.5b02303
ACS Appl. Mater. Interfaces 2015, 7, 10977−10987

commonly grown on CuNPs. In order to obtain monolayer graphene on CuNPs, the H_2/CH_4 ratio was tuned. The monolayer graphene with low level of defect was achieved with 50 sccm H_2 and 10 sccm CH_4 (Figures S6 and S7, in the SI). This optimal ratio of the two gases could be possibly determined by the dual role of hydrogen in the process of graphene growth by CVD on copper with methane as a carbon source. The hydrogen acts as a cocatalyst in improving graphene quality and suppressing the muti-layer structure by etching away the "weak" carbon−carbon bonds. On the other hand, the excess hydrogen will also destroy the existing graphene, increasing the defect-level of graphene. To achieve the balance of these two competition processes could be the critical for high-quality monolayer graphene.

Fabrication of CuNPs on Flat Quartz Substrate. For CuNPs fabrication, the whole procedure was similar to that of G/CuNPs fabrication. The difference here is that when the high-temperature zone reached 1050 °C the mixture of 50 sccm H_2 and 150 sccm Ar at 1350 Pa was replaced by 50 sccm H_2 and 10 sccm Ar at 280 Pa (Figure S8, SI). After 5 min reaction, the CuNPs were deposited onto the flat quartz substrate in the low-temperature zone.

Fabrication of TG/CuNPs. The CVD monolayer graphene was grown on 25 μm Cu foil at 1050 °C with flowing of 60 and 15 sccm by using the growth procedure in our recent report.[65] A 200 nm-thick PMMA was deposited onto the graphene film by the spin-coated method, and then the Cu foil was etched away by 0.5 M aqueous $FeCl_3$ solution. After removing the residual etchant in deionized water, the PMMA-coated graphene films were transferred onto the CuNPs layer. In order to relax the underlying graphene, a second PMMA coating was introduced onto the precoated PMMA layer. Then, the whole PMMA layer was dissolved with acetone, forming the TG/CuNPs structure. Finally, the TG/CuNPs were dried at 50 °C for 30 min with flowing 100 sccm Ar to evaporate the solvent completely.

Thermal Oxidation Treatment. For thermal oxidation treatment, the G/CuNPs, TG/CuNPs, and CuNPs were placed onto the 85 °C hot plate in a glovebox connected with atmosphere. A humidifier runs intermittently according to feedback from a humidity sensor to keep the glovebox humidity of 80%. The thermal oxidation treatment was performed for 240 h.

Preparation of Urine Samples. The single, early morning urine samples were provided by Department of Internal Medicine of Dezhou People's Hospital from ten healthy volunteers (physical examination people). The samples were centrifuged at a speed of 10 000 rpm for 10 min and the upper liquid was collected for Raman measurements. The nucleosides were extracted from urines by affinity chromatography using a phenylboronic acid gel (Affi-gel 601) in a glass column. After the gel was activated and equilibrated with 20 mL of 0.1 M NH_4OAc, 1 mL centrifuged urine was applied to the column. Then the gel was washed with 10 mL of 0.1 M NH_4OAc and 10 mL of methanol−water (1:1, *v*/*v*). The nucleosides were eluted with 10 mL of 0.05 M HCOOH in methanol−water (1:1, *v*/*v*). Finally, the nucleoside solution was enriched to 1 mL by evaporation for Raman measurements.

SERS Experiments. SERS experiments were carried out using a Raman system (Horiba HR-800) with laser excitation at 532 nm (2.33 eV). The excitation laser spot was about 0.5 μm, and the incident laser power was kept at 0.5 mW. The system was connected to a microscope, and the laser light was coupled through an objective lens of 20× , which was used for exciting the sample as well as collecting the Raman signals. Prior to each Raman experiment, calibration of the instrument was done with the Raman signal from a silicon standard centered at 520 cm^{-1}. Subtraction of the baseline using cubic spline interpolation was performed in order to eliminate unwanted background noise and to facilitate data analysis. SERS substrates were incubated for 2.5 h in different analyte solutions at 25 °C. Substrates were taken out and fixed onto the glass slide. SERS measurements were taken from at least eight random locations that were more than 3 mm apart with an accumulation time of 30 s. If there is no special instruction, the mentioned Raman spectra are expressed in terms of average spectra.

Apparatus and Characterization. The Raman spectroscopy of graphene was performed using a Raman spectrometer (Horiba HR-800) with laser excitation at 532 nm (2.33 eV). Surface morphologies of G/CuNPs, TG/CuNPs, and CuNPs were observed using a SEM (Hitachi S-570). The HRTEM images of G/CuNPs were obtained using a transmission electron microscopy system (JEOL, JEM-2100) operated at 100 kV. The surface compositions of G/CuNPs, TG/CuNPs, and CuNPs were characterized by XRD (Rigaku D/MAX-RB). XPS was carried out on a VGESCA Lab-250 using Al Kα X-rays as the excitation source. Curve fitting of the spectra was carried out using a Lorentzian peak shape.

■ ASSOCIATED CONTENT

Ⓢ Supporting Information

TEM of CuNPs; XRD, SEM, EDS, and XPS after thermal oxidation treatment; the linear SERS responses versus concentration of adenosine from TG/CuNPs and CuNPs; experimental procedure for fabrication of G/CuNPs and CuNPs; the analysis of effect of the H_2/CH_4 ratio used for graphene growth including Raman spectra and Raman mappings. The Supporting Information is available free of charge on the ACS Publications website at DOI: 10.1021/acsami.5b02303.

■ AUTHOR INFORMATION

Corresponding Author

*E-mail: xushicai001@163.com; shicaixu@dzu.edu.cn. Tel: +86 534 8982081.

Notes

The authors declare no competing financial interest.

■ ACKNOWLEDGMENTS

The authors are grateful for financial support from the Shandong Province Natural Science Foundation (ZR2014FQ032 and ZR2013HL049) and the National Natural Science Foundation of China (11474187 and 61205174).

■ REFERENCES

(1) Barhoumi, A.; Halas, N. J. Label-Free Detection of DNA Hybridization Using Surface Enhanced Raman Spectroscopy. *J. Am. Chem. Soc.* **2010**, *132*, 12792−12793.

(2) Lee, K.; Drachev, V. P.; Irudayaraj, J. DNA Gold Nanoparticle Reversible Networks Grown on Cell Surface Marker Sites: Application in Diagnostics. *ACS Nano* **2011**, *5*, 2109−2117.

(3) Wang, Y.; Wei, H.; Li, B.; Ren, W.; Guo, S.; Dong, S.; Wang, E. SERS Opens a New Way in Aptasensor for Protein Recognition with High Sensitivity and Selectivity. *Chem. Commun.* **2007**, *48*, 5220−5222.

DOI: 10.1021/acsami.5b02303
ACS Appl. Mater. Interfaces 2015, 7, 10977−10987

(4) Fan, M.; Andrade, G. F. S.; Brolo, A. G. A Review on the Fabrication of Substrates for Surface Enhanced Raman Spectroscopy and Their Applications in Analytical Chemistry. *Anal. Chim. Acta* **2011**, *693*, 7−25.
(5) Cialla, D.; März, A.; Böhme, R.; Theil, F.; Weber, K.; Schmitt, M.; Popp, J. Surface-Enhanced Raman Spectroscopy (SERS): Progress and Trends. *Anal. Bioanal. Chem.* **2012**, *403*, 27−54.
(6) Banholzer, M. J.; Millstone, J. E.; Qin, L.; Mirkin, C. A. Rationally Designed Nanostructures for Surface-Enhanced Raman Spectroscopy. *Chem. Soc. Rev.* **2008**, *37*, 885−897.
(7) Li, J. F.; Huang, Y. F.; Ding, Y.; Yang, Z. L.; Li, S. B.; Zhou, X. S.; Fan, F. R.; Zhang, W.; Zhou, Z. Y.; Wu, D. Y.; Ren, B.; Wang, Z. L.; Tian, Z. Q. Shell-Isolated Nanoparticle-Enhanced Raman Spectroscopy. *Nature* **2010**, *464*, 392−395.
(8) Yao, H.; Jin, L.; Sue, H. J.; Sumi, Y.; Nishimura, R. Facile Decoration of Au Nanoparticles on Reduced Graphene Oxide Surfaces via A One-Step Chemical Functionalization Approach. *J. Mater. Chem. A* **2013**, *1*, 10783−10789.
(9) Zheng, J.; Li, X.; Gu, R.; Lu, T. Comparison of the Surface Properties of the Assembled Silver Nanoparticle Electrode and Roughened Silver Electrode. *J. Phys. Chem. B* **2002**, *106*, 1019−1023.
(10) Novoselov, K. S.; Geim, A. K.; Morozov, S. V.; Jiang, D.; Zhang, Y.; Dubonos, S. V.; Grigorieva, I. V.; Firsov, A. A. Electric Field Effect in Atomically Thin Carbon Films. *Science* **2004**, *306*, 666−669.
(11) Geim, A. K.; Novoselov, K. S. The Rise of Graphene. *Nat. Mater.* **2007**, *6*, 183−191.
(12) Freebody, M. Preserving Moore's Law Pushes Lithography to Its Limits. *Photonics Spectra* **2010**, *44*, 25−26.
(13) Balandin, A. A.; Ghosh, S.; Bao, W.; Calizo, I.; Teweldebrhan, D.; Miao, F.; Lau, C. N. Superior Thermal Conductivity of Single-Layer Graphene. *Nano Lett.* **2008**, *8*, 902−907.
(14) Yang, H.; Hu, H.; Ni, Z.; Poh, C. K.; Cong, C.; Lin, J.; Yu, T. Comparison of Surface-Enhanced Raman Scattering on Graphene Oxide, Reduced Graphene Oxide and Graphene Surfaces. *Carbon* **2013**, *62*, 422−429.
(15) Xu, W.; Mao, N.; Zhang, J. Graphene: A Platform for Surface Enhanced Raman Spectroscopy. *Small* **2013**, *9*, 1206−1224.
(16) Xie, L.; Ling, X.; Fang, Y.; Zhang, J.; Liu, Z. Graphene as a Substrate to Suppress Fluorescence in Resonance Raman Spectroscopy. *J. Am. Chem. Soc.* **2009**, *131*, 9890−9891.
(17) Ling, X.; Zhang, J. Interference Phenomenon in Graphene Enhanced Raman Scattering. *J. Phys. Chem. C* **2011**, *115*, 2835−2840.
(18) Zhang, Z.; Xu, F.; Yang, W.; Guo, M.; Wang, X.; Zhang, B.; Tang, J. A Facile One-Pot Method to High-Quality Ag-Graphene Composite Nanosheets for Efficient Surface-Enhanced Raman Scattering. *Chem. Commun.* **2011**, *47*, 6440−6442.
(19) He, S.; Liu, K. K.; Su, S.; Yan, J.; Mao, X.; Wang, D.; He, Y.; Li, L. J.; Song, S.; Fan, C. Graphene Based High-Efficiency Surface-Enhanced Raman Scattering Active Platform for Sensitive and Multiplex DNA detection. *Anal. Chem.* **2012**, *84*, 4622−4627.
(20) Xie, Y.; Li, Y.; Niu, L.; Wang, H.; Qian, H.; Yao, W. A Novel Surface Enhanced Raman Scattering Sensor to Detect Prohibited Colorants in Food by Graphene/Silver Nanocomposite. *Talanta* **2012**, *100*, 32−37.
(21) Zhao, H.; Fu, H.; Zhao, T.; Wang, L.; Ta, T. Fabrication of Small-Sized Silver NPs/Graphene Sheets for High-Quality Surface Enhanced Raman Scattering. *J. Colloid Interface Sci.* **2012**, *375*, 30−34.
(22) Iliut, M.; Leordean, C.; Canpean, V.; Teodorescu, C. M.; Astilean, S. A New Green, Ascorbic Acid-Assisted Method for Versatile Synthesis of Au−Graphene Hybrids as Efficient Surface Enhanced Raman Scattering Platforms. *J. Mater. Chem. C* **2013**, *1*, 4094−4104.
(23) Liu, M.; Chen, W. Graphene Nanosheets-Supported Ag Nanoparticles for Ultrasensitive Detection of TNT by Surface Enhanced Raman Spectroscopy. *Biosens. Bioelectron.* **2013**, *46*, 68−73.
(24) Lu, R.; Konzelmann, A.; Xu, F.; Gong, Y.; Liu, J.; Liu, Q.; Xin, M.; Hui, R.; Wu, J. Z. High Sensitivity Surface Enhanced Raman Spectroscopy of R6G on in situ Fabricated Au Nanoparticle/Graphene Plasmonic Substrates. *Carbon* **2015**, *86*, 78−85.
(25) Xu, W.; Xiao, J.; Chen, Y.; Chen, Y.; Ling, X.; Zhang, J. Graphene Veiled Gold Substrate for Surface-Enhanced Raman Spectroscopy. *Adv. Mater.* **2013**, *25*, 928−933.
(26) Wang, P.; Liang, O.; Zhang, W.; Schroeder, T.; Xie, Y. H. Ultra-Sensitive Graphene-Plasmonic Hybrid Platform for Label-Free Detection. *Adv. Mater.* **2013**, *25*, 4918−4924.
(27) Du, Y.; Zhao, Y.; Qu, Y.; Chen, C. H.; Chen, C. M.; Chuang, C. H.; Zhu, Y. Enhanced Light−Matter Interaction of Graphene−Gold Nanoparticle Hybrid Films for High-Performance SERS Detection. *J. Mater. Chem. C* **2014**, *2*, 4683−4691.
(28) Li, X.; Li, J.; Zhou, X.; Ma, Y.; Zheng, Z.; Duan, X.; Qu, Y. Silver Nanoparticles Protected by Monolayer Graphene as a Stabilized Substrate for Surface Enhanced Raman Spectroscopy. *Carbon* **2014**, *66*, 713−719.
(29) Li, X.; Cai, W.; An, J.; Kim, S.; Nah, J.; Yang, D.; Richard, P.; Aruna, V.; Inhwa, J.; Emanuel, T.; Sanjay, K. B.; Luigi, C.; Ruoff, R. S. Large-Area Synthesis of High-Quality and Uniform Graphene Films on Copper Foils. *Science* **2009**, *324*, 1312−1314.
(30) Dulla, C. G.; Masino, S. A. Physiologic and Metabolic Regulation of Adenosine: Mechanisms. *Adenosine*; Springer: New York, 2013; pp 87−107.
(31) Xu, F.; Wu, H.; Katritch, V.; Han, G. W.; Jacobson, K. A.; Gao, Z. G.; Cherezov, V.; Stevens, R. C. Structure of an Agonist-Bound Human A2A Adenosine Receptor. *Science* **2011**, *332*, 322−327.
(32) Lebon, G.; Warne, T.; Edwards, P. C.; Bennett, K.; Langmead, C. J.; Leslie, A. G.; Tate, C. G. Agonist-Bound Adenosine A2A Receptor Structures Reveal Common Features of GPCR Activation. *Nature* **2011**, *474*, 521−525.
(33) Zheng, Y. F.; Yang, J.; Zhao, X. J.; Feng, B.; Kong, H. W.; Chen, Y. J.; Lv, S.; Zheng, M. H.; Xu, G. W. Urinary Nucleosides as Biological Markers for Patients with Colorectal Cancer. *World J. Gastroenterol.* **2005**, *11*, 3871−3876.
(34) Hsu, W. Y.; Lin, W. D.; Tsai, Y.; Lin, C. T.; Wang, H. C.; Jeng, L. B.; Leee, C. C.; Line, Y. C.; Laic, C. C.; Tsai, F. J. Analysis of Urinary Nucleosides as Potential Tumor Markers in Human Breast Cancer by High Performance Liquid Chromatography/Electrospray Ionization Tandem Mass Spectrometry. *Clin. Chim. Acta* **2011**, *412*, 1861−1866.
(35) Jeng, L. B.; Lo, W. Y.; Hsu, W. Y.; Lin, W. D.; Lin, C. T.; Lai, C. C.; Tsai, F. J. Analysis of Urinary Nucleosides as Helper Tumor Markers in Hepatocellular Carcinoma Diagnosis. *Rapid Commun. Mass Spectrom.* **2009**, *23*, 1543−1549.
(36) Mcleod, A.; Vernon, K. C.; Rider, A. E.; Ostrikov, K. Optical Coupling of Gold Nanoparticles on Vertical Graphenes to Maximize SERS Response. *Opt. Lett.* **2014**, *39*, 2334−2337.
(37) Ferrari, A. C.; Meyer, J. C.; Scardaci, V.; Casiraghi, C.; Lazzeri, M.; Mauri, F.; Piscanec, S.; Jiang, D.; Novoselov, K. S.; Roth, S.; Geim, A. K. Raman Spectrum of Graphene and Graphene Layers. *Phys. Rev. Lett.* **2006**, *97*, 187401.
(38) Ferrari, A. C. Raman Spectroscopy of Graphene and Graphite: Disorder, Electron−Phonon Coupling, Doping and Nonadiabatic Effects. *Solid State Commun.* **2007**, *143*, 47−57.
(39) Xu, S. C.; Man, B. Y.; Jiang, S. Z.; Chen, C. S.; Yang, C.; Liu, M.; Gao, X. G.; Sun, Z. C.; Zhang, C. Direct Synthesis of Graphene on SiO_2 Substrates by Chemical Vapor Deposition. *CrystEngComm* **2013**, *15*, 1840−1844.
(40) Xu, S. C.; Man, B. Y.; Jiang, S. Z.; Liu, M.; Yang, C.; Zhang, C. Graphene− Silver Nanowire Hybrid Films as Electrodes for Transparent and Flexible Loudspeakers. *CrystEngComm* **2014**, *16*, 3532−3539.
(41) Singh, A. K.; Khan, S. A.; Fan, Z.; Demeritte, T.; Senapati, D.; Kanchanapally, R.; Ray, P. C. Development of a Long-Range Surface-Enhanced Raman Spectroscopy Ruler. *J. Am. Chem. Soc.* **2012**, *134*, 8662−8669.
(42) Meyer, J. C.; Geim, A. K.; Katsnelson, M. I.; Novoselov, K. S.; Booth, T. J.; Roth, S. The structure of suspended graphene sheets. *Nature* **2007**, *446*, 60−63.
(43) Xu, S. C.; Man, B. Y.; Jiang, S. Z.; Liu, A. H.; Hu, G. D.; Chen, C. S.; Liu, M.; Yang, C.; Feng, D. J.; Zhang, C. Direct Synthesis of

DOI: 10.1021/acsami.5b02303
ACS Appl. Mater. Interfaces 2015, 7, 10977−10987

Graphene on Any Nonmetallic Substrate Based on KrF Laser Ablation of Ordered Pyrolytic Graphite. *Laser Phys. Lett.* **2014**, *11*, 096001.
(44) Hernandez, Y.; Nicolosi, V.; Lotya, M.; Blighe, F. M.; Sun, Z.; De, S.; Mcgovern, I. T.; Holland, B.; Byrne, M.; Gun'ko, Y. K.; Boland, J. J.; Niraj, P.; Duesberg, G.; Krishnamurthy, S.; goodhue, R.; Hutchison, J.; Scardaci, V.; Ferrari, A. C.; Coleman, J. N. High-Yield Production of Graphene by Liquid-Phase Exfoliation of Graphite. *Nat. Nanotechnol.* **2008**, *3*, 563−568.
(45) Zhang, C.; Man, B. Y.; Yang, C.; Jiang, S. Z.; Liu, M.; Chen, C. S.; Xu, S. C.; Sun, Z. C.; Gao, X. G. Facile Synthesis of Graphene on Dielectric Surfaces Using a Two-Temperature Reactor Cvd System. *Nanotechnology* **2013**, *24*, 395603.
(46) Chen, J.; Wen, Y.; Guo, Y.; Wu, B.; Huang, L.; Xue, Y.; Geng, D.; Wang, D.; Yu, G.; Liu, Y. Oxygen-Aided Synthesis of Polycryst alline Graphene on Silicon Dioxide Substrates. *J. Am. Chem. Soc.* **2011**, *133*, 17548−17551.
(47) Tien, H. W.; Huang, Y. L.; Yang, S. Y.; Wang, J. Y.; Ma, C. C. M. The Production of Graphene Nanosheets Decorated with Silver Nanoparticles for Use in Transparent, Conductive Films. *Carbon* **2011**, *49*, 1550−1560.
(48) Bae, S.; Kim, H.; Lee, Y.; Xu, X.; Park, J. S.; Zheng, Y.; Balakrishnan, J.; Lei, T.; Kim, H. R.; Song, Y. I.; Kim, Y. J.; Kim, K. S.; Özyilmaz, B.; Ahn, J. H.; Hong, B. H.; Iijima, S. Roll-to-Roll Production of 30-Inch Graphene Films for Transparent Electrodes. *Nat. Nanotechnol.* **2010**, *5*, 574−578.
(49) Medina, H.; Lin, Y. C.; Jin, C.; Lu, C. C.; Yeh, C. H.; Huang, K. P.; Suenaga, K.; Robertson, J.; Chiu, P. W. Metal-Free Growth of Nanographene on Silicon Oxides for Transparent Conducting Applications. *Adv. Funct. Mater.* **2012**, *22*, 2123−2128.
(50) Giese, B.; McNaughton, D. Surface−Enhanced Raman Spectroscopic and Density Functional Theory Study of Adenine Adsorption to Silver Surfaces. *Phys. Chem. B* **2002**, *106*, 101−112.
(51) Li, J.; Fang, Y. An Investigation of the Surface Enhanced Raman Scattering (SERS) from a New Substrate of Silver−Modified Silver Electrode by Magnetron Sputtering. *Spectrochim. Acta, Part A* **2007**, *66*, 994−1000.
(52) Giese, B.; McNaughton, D. Surface−enhanced Raman Spectroscopic and Density Functional Theory Study of Adenine Adsorption to Silver Surfaces. *Phys. Chem. B* **2002**, *106*, 101−112.
(53) Talari, A. C. S.; Movasaghi, Z.; Rehman, S.; Rehman, I. U. Raman Spectroscopy of Biological Tissues. *Appl. Spectrosc. Rev.* **2015**, *50*, 46−111.
(54) Chen, A.; Long, H.; Li, X.; Li, Y.; Yang, G.; Lu, P. Controlled Growth and Characteristics of Single-Phase Cu_2O and CuO Films by Pulsed Laser Deposition. *Vacuum* **2009**, *83*, 927−930.
(55) Chusuei, C. C.; Brookshier, M. A.; Goodman, D. W. Correlation of Relative X-ray Photoelectron Spectroscopy Shake-up Intensity with CuO Particle Size. *Langmuir* **1999**, *15*, 2806−2808.
(56) Chen, J. W.; Liu, X. P.; Feng, K. J.; Liang, Y.; Jiang, J. H.; Shen, G. L.; Yu, R. Q. Detection of Adenosine Using Surface-Enhanced Raman Scattering Based on Structure-Switching Signaling Aptamer. *Biosens. Bioelectron.* **2008**, *24*, 66−71.
(57) Zhang, W.; Qiu, T.; Qu, X. P.; Chu, P. K. Atomic Layer Deposition of Platinum Thin Films on Anodic Aluminium Oxide Templates as Surface-Enhanced Raman Scattering Substrates. *Vacuum* **2013**, *89*, 257−260.
(58) Li, B.; Du, Y.; Wei, H.; Dong, S. Reusable, Label-free Electrochemical Aptasensor for Sensitive Detection of Small Molecules. *Chem. Commun.* **2007**, *36*, 3780−3782.
(59) Yan, X.; Cao, Z.; Kai, M.; Lu, J. Label-Free Aptamer-Based Chemiluminescence Detection of Adenosine. *Talanta* **2009**, *79*, 383−387.
(60) Cheng, W. T.; Liu, M. T.; Liu, H. N.; Lin, S. Y. Micro-Raman Spectroscopy Used to Identify and Grade Human Skin Pilomatrixoma. *Microsc. Res. Technol.* **2005**, *68*, 75−79.
(61) Malini, R.; Venkatakrishna, K.; Kurien, J.; M Pai, K.; Rao, L.; Kartha, V. B.; Krishna, C. M. Discrimination of Normal, Inflammatory, Premalignant, and Malignant Oral Tissue: a Raman Spectroscopy Study. *Biopolymers* **2006**, *81*, 179−193.
(62) Ruiz-Chica, A. J.; Medina, M. A.; Sanchez-Jimenez, F.; Ramirez, F. J. Characterization by Raman Spectroscopy of Conformational Changes on Guanine-Cytosine and Adenine-Thymine Oligonucleotides Induced by Aminooxy Analogues of Spermidine. *J. Raman Spectrosc.* **2004**, *35*, 93−100.
(63) Shapiro, A.; Gofrit, O. N.; Pizov, G.; Cohen, J. K.; Maier, J. Raman Molecular Imaging: a Novel Spectroscopic Technique for Diagnosis of Bladder Cancer in Urine Specimens. *Eur. Urol.* **2011**, *59*, 106−112.
(64) Kiraly, B.; Iski, E. V.; Mannix, A. J.; Fisher, B. L.; Hersam, M. C.; Guisinger, N. P. Solid−Source Growth and Atomic-Scale Characterization of Graphene on Ag(111). *Nat. Commun.* **2013**, *4*, 2804.
(65) Xu, S. C.; Man, B. Y.; Jiang, S. Z.; Chen, C. S.; Yang, C.; Liu, M.; Gao, X. G.; Sun, Z. C.; Zhang, C. Flexible and Transparent Graphene−Based Loudspeakers. *Appl. Phys. Lett.* **2013**, *102*, 151902.

DOI: 10.1021/acsami.5b02303
ACS Appl. Mater. Interfaces 2015, 7, 10977−10987